Kapal: Jurnal Ilmu Pengetahuan dan Teknologi Kelautan
(Kapal: Journal of Marine Science and Technology)

2301-9069 (e)
1829-8370 (p)

journal homepage : http://ejournal.undip.ac.id/index.php/kapal

# Numerical Investigation on The Open Water Characteristics of B-Series Propeller

Andik Machfudin[1) 2)], A.A.B. Dinariyana[2)*)], Dian Purnama Sari[2)]

[1)] Department of Marine Engineering, Institut Teknologi Sepuluh Nopember, Surabaya, Indonesia
[2)] National Research and Innovation Agency, Indonesia
[*)] Corresponding Author: dinariyana@yahoo.com

**Article Info**

**Keywords:**
Open Water Characteristics;
CFD, Propeller;
Mesh Convergence;
Advance Coefficient;

**Article history:**
Received: 23/05/2023
Last revised: 27/06/2023
Accepted: 28/06/2023
Available online: 28/06/2023
Published: 30/06/2023

**DOI:**
https://doi.org/10.14710/kapal.v20i2.54507

**Abstract**

Computer fluid dynamics (CFD) has been increasingly popular in the present day attributable to the reasonably accurate results, time and money savings, and ease of use for calculating the open water characteristics of the propeller. This paper presents the results of a computational evaluation of propeller open water characteristics based on various advanced velocities and advanced coefficients. $K_T$, $K_Q$, and $\eta$ are verified to get optimal performance study results. Research on mesh convergence is conducted with an advance coefficient of $J = 0.6$ with investigate three meshes coarse, medium, and fine. The impacts of mesh density and mesh production are examined for the purpose of increasing the accuracy of the numerical findings. The B-series propeller is used to verify and validate the accuracy of case studies. Obtained results show that the CFD result is well in agreement with the experimental result.



## 1. Introduction

The performance of propellers is constantly being researched in the design for methods to increase their effectiveness, noise level, and erosion. Model testing and Computational Fluid Dynamics (CFD) simulations are the standard procedures for determining the performance of propellers. A propeller is examined in an open-water performance study under wet and cavitation flow conditions. Data on thrust, torque coefficient, and efficiency are produced for a range of advanced ratio values. For the purpose of ensuring data consistency, experimental and CFD results are compared.

Various mesh and computation domains are the main parameters in the simulation method. Based on analyzing the effects of different mesh and computation domain parameters, researchers suggest mesh and domain optimization strategies for a common CFD technique to accurately and quickly estimate the open water propulsive characteristics of fixed pitch propellers [1]. An accurate predictive technique is needed to produce enough power and torque to move the ship forward at the necessary speed [2]. The study of a maritime propeller from a bulk carrier is verified to obtain an energy-saving device (ESD). When used in many domains, Propeller Boss Cap Fins (PBCF) could enhance thrust, reduce torque and boost efficiency [3].

The Simulation of the propeller conclude that the magnitude of the $K_T$ and $K_Q$ of the propeller had a direct correlation with the subsequent increase in blade numbers [4]. The study uses a CFD approach to examine a smooth and roughened hull of the ship caused by marine biofouling and it showed that marine biofouling significantly increases ship resistance [5]. There are large-scale effects on open water properties; however, when the transition model is used in numerical simulations at the model scale, there are much smaller scale effects [6]. In order to validate numerical simulations of the static hydroelastic response of marine propellers, tests were conducted. The test matrix allows testing of design and simulation codes against the effects of Reynolds number, skew distribution, and the static hydroelastic response of resin propellers in open water [7]. An inspection of an underground gas pipeline revealed anomalous examples of wall distortion, and the findings were used to conduct a stress analysis using finite element analysis under three different bedding conditions [8].

The CFD simulation and the experimental tank test showed good agreement to demonstrate how extra resistance and power in waves increased in comparison to a calm water situation [9]. The impact of distance from the seabed on the drag and lift of the submarine is examined using the CFD approach and indicated that the distance-diameter ratio has a somewhat negative impact on the drag force but a considerable positive impact on the lift force. The negative lift increases with distance from the seafloor, which can pull the submarine in so that it strikes the bottom [10]. The different grid types, mesh densities, and turbulence models affect the outcomes of the simulation [11]. The Schnerr-Sauer cavitation model is used to conduct numerical examinations of the cavitation and hydrodynamic properties of propellers in uniform and non-uniform flows [12].

Propeller simulation also is also verified to research the interaction with the ship hull or rudder. a series of numerical simulations based on RANSE are performed to explore the propeller characteristics in near-field contact between ships at rest [13]. The unstable interaction between the propeller and rudder is simulated using a numerical technique based on a potential flow method [14]. a comparison between sea trial measurements and full-scale CFD findings is researched For two separate self-propelled ships with various Froude values [15]. In real-world maritime situations, waves cause ship hulls to heave, which can cause the ship's propellers to oscillate in relation to the surrounding sea [16].

The rudder surface may vibrate as a result of the propeller wake, which will increase noise and dependability. Detached eddy simulation is used to examine the structural reaction during propeller-rudder interaction [17]. Using large eddy simulation, the evolution of the propeller tip vortex and its impact on the variation of the rudder surface pressure were examined [18]. Meanwhile, four sets of progressively finer grids are used to conduct a grid-dependence analysis of the large-eddy simulation (LES) with the immersed boundary (IB) approach for simulating a propeller in crash-back mode [19]. The large-eddy simulations are used to study the open water of a submarine propeller [20] and obtained the result results of the first high-order eddy-resolving simulation of flow over a maritime propeller [21].

The objective of this study is to conduct numerous numerical simulations of the B-series propeller to determine the hydrodynamic force based on modifications in the advance velocity (Va), which will change the advance coefficient. Research on mesh convergence is conducted with an advance coefficient of $J$ = 0.6. Three meshes coarse, medium, and fine are generated with cell counts of 1.38, 3.52, and 6.89 million. According to the available research, no numerical analysis utilizing Numeca Fine Marine has ever been done to determine the parameters of the open water test of this particular type of propeller. The auto-mesh settings selected in this software set it apart from other software.

## 2. Methods

CFD is the term for the computer-based simulation-based analysis of systems containing fluid flow, heat transport, and similar phenomena. A hydrodynamic design was used to create the propeller. Given that water is both an incompressible fluid and a Newtonian fluid, the incompressible Navier-Stokes equations are applicable as in Eq. 1 and 2.

$$\frac{\partial}{\partial x_j}\left(U_j U_i\right) = -\frac{1}{\rho}\frac{\partial P}{\partial x_i} + v\frac{\partial^2 U_i}{\partial x_j x_i} \tag{1}$$

$$\frac{\partial U_j}{\partial U_x} = 0 \tag{2}$$

Extreme computer power is required to answer this set of equations. It is desirable to divide the pressure and velocities into a mean and a fluctuating fraction, as in Eq.3, because the flow is turbulent. Reynolds decomposition is the term for this.

$$U_i = \bar{U}_i + u_i$$

$$P = \bar{P} + p \tag{3}$$

where U is velocity and P is pressure. The Reynolds-Averaged Navier-Stokes and continuity equation are produced by adding Eq. 3 into Eq. 1 and 2. It is shown in Eq. 4 and 5.

$$\frac{\partial}{\partial x_j}\left(\bar{U}_i \bar{U}_j\right) = -\frac{1}{\rho}\frac{\partial \bar{P}}{\partial x_i} v\frac{\partial^2 U_i}{\partial x_i \partial x_j} - \frac{\partial \overline{u_i u_j}}{\partial x_j} \tag{4}$$

$$\frac{\partial \bar{U}_j}{\partial x_j} = 0 \tag{5}$$

The model scale propeller is operated in a uniform inflow through the open water test. This might be carried out in a cavitation tunnel or a towing tank. Typically, the advance velocity ($Va$) is changed for a fixed number of revolutions per second ($n$) during the test and the propeller thrust ($T$) and propeller torque ($Q$) are measured. The relationship between $Va$ and the velocity ($Va$) in the tangential direction, which gives an indicator of the angle of attack for the blade profiles, must be the same to obtain the identical conditions in full scale as in model scale. The advance ratio ($J$) and $V$ are defined as follows in Eq. 6.

$$J = \frac{Va}{nD} \tag{6}$$

The definitions of the non-dimensional quantities $K_T$, $K_Q$, and $\eta_o$ are given in Eq.7, 8, and 9.

$$K_T = \frac{T}{\rho n^2 D^5} \tag{7}$$

$$K_Q = \frac{Q}{\rho n^2 D^5} \tag{8}$$

$$\eta_o = \frac{JK_T}{2\pi K_Q} \tag{9}$$

$K_T$ = coefficient thrust, $K_Q$ = coefficient torque, $\rho$ = fluid density, and $\eta_O$ = open water efficiency

The open water characteristics are the measurements that are typically made in the open water test, which are denoted by the letters $K_T$, $K_Q$, and $\eta_o$. The open water chart is produced by comparing them to *J*. Since they should be same in a model and at full scale, these qualities are of interest.

### 2.1. Propeller Model

The software NUMECA FINE/ Marine 7.2 was used to create a computational model of propeller performance in various configurations. Different rotating speeds were employed to study in this paper. Table 1 and Figure 1 clearly display the propeller's main dimensions, which are made up of four blades.

Table 1. The propeller's main dimensions.

| No. | Parameter | Value |
|---|---|---|
| 1 | Propeller | B-Series |
| 2 | Number of blades (*Z*) | 4 |
| 3 | Diameter (*D*) | 157.6 mm |
| 4 | Propeller Pitch ratio (*P/D*) | 1.133 |
| 6 | Pitch 0.7 *R* | 178.6 mm |
| 7 | Blade Area Ration ($A_E/A_o$) | 0.65 |
| 8 | Rotation | Right Hand |

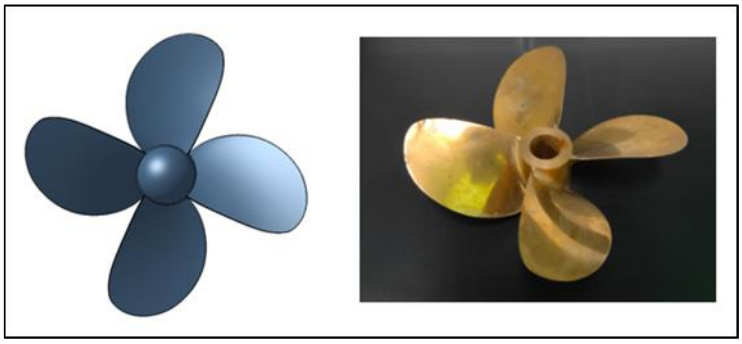

Figure 1. The geometry of the propeller.

### 2.2. Modeling Configuration

This open water simulation's computation process is identical to that of an experiment. The advance coefficient J has an interval of 0.0 to 1.2 with a 0.1 stage. This means that altering advance velocity (*Va*) will alter the advance coefficient (*J*). Water density =998.67 kg/m$^3$ and kinematic viscosity $v$ = 1.070.10-6 m$^2$/s are the environmental variables that correspond to the experimental setup. The trailing edge, leading edge, pressure side, suction side, and hub of the propeller must all be defined in the geometry of the four propeller blades in order to create an automatic grid. Figure 2 shows the characteristics of the propeller geometry.

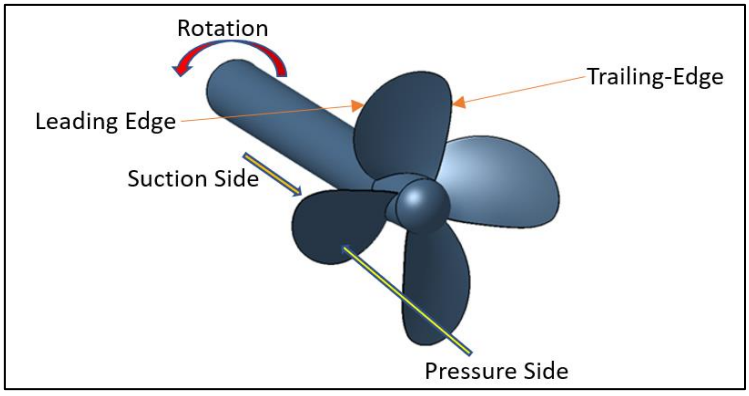


Figure 2. The characteristics of the propeller geometry

### 2.3. Meshing

It is important to remember that for proper and accurate simulation, an adequate number of meshes is crucial. A mesh-independent analysis may therefore need to be carried out for three alternative total numbers of cell meshing. Figures 3, 4, and 5 show the final coarse, medium, and fine mesh for the propeller's open water test. The distribution of cells is the most notable variation, as can be observed. The fine mesh considerably improves the resolution around the propeller and in the

slipstream. For the fine mesh as well, the cells in the domain region are a little bit bigger. The cells near the domain walls are marginally smaller than the free-stream cells.

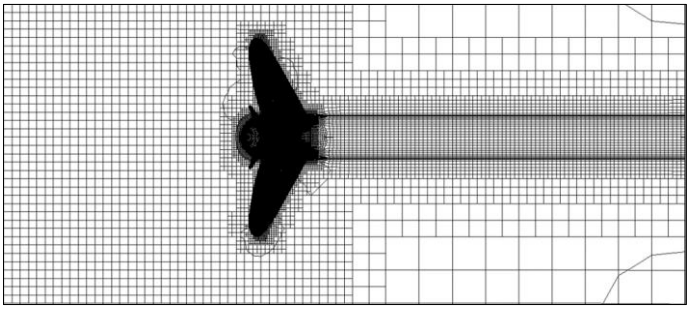

Figure 3. The generated mesh of the propeller (course).

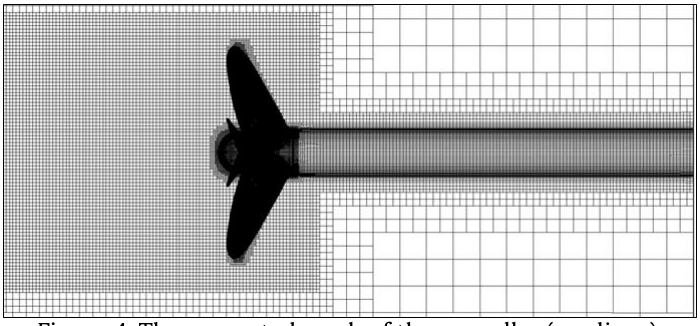

Figure 4. The generated mesh of the propeller (medium).

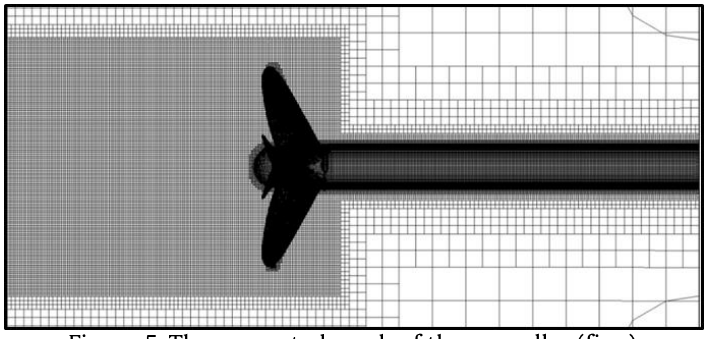

Figure 5. The generated mesh of the propeller (fine).

### 2.4. Setting Up

The cylinder's side is designated as the symmetry plane, and the boundary conditions are velocity inlet at the inlet; outlet pressure at the outlet. With advance velocity proportional to advance coefficient ($J$), the flow velocity is enforced at the inlet. The hub, shaft, and propeller blades are hence designated as the "wall" boundary. The diameter of a propeller is the cylinder that serves as the computation domain. The outlet boundary has been extended to five times the propeller diameter (5D) in order to prevent the effects of the boundary and to effectively capture the propeller vortex. The outlet boundary is two times the propeller diameter (2D) away from the propeller plane and the domain's diameter (3D) is three times that of a propeller. It needs to be noticed that the boundaries' placement was chosen based on suggestions made by the ITTC. Figure 6 displays the scheme of the computational domain.

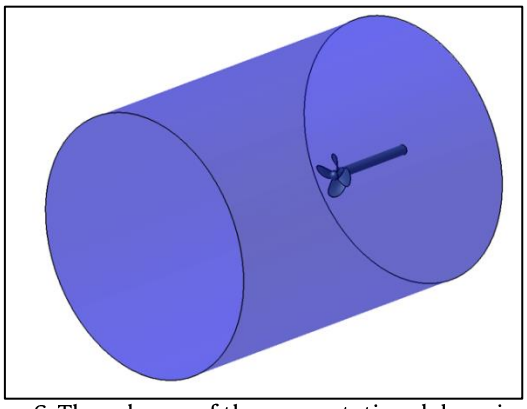

Figure 6. The scheme of the computational domain.

### 2.5. Simulation Condition

Numerous numerical simulations were conducted in this study to determine the hydrodynamic force based on modifications in the advance velocity (*Va*), which will change the advance coefficient (*J*), as shown in Table 2. Research on mesh convergence is conducted with an advance coefficient of *J* = 0.6. Three meshes coarse, medium, and fine are generated with cell counts of 1.38, 3.52, and 6.89 million.

Table 2. Numerical simulation condition.

| *J* | *Va(m/s)* | *Rps* |
|---|---|---|
| 0.0 | 0.00 | 22.016 |
| 0.1 | 0.347 | 22.016 |
| 0.2 | 0.694 | 22.016 |
| 0.3 | 1.041 | 22.016 |
| 0.4 | 1.388 | 22.016 |
| 0.5 | 1.735 | 22.016 |
| 0.6 | 2.082 | 22.016 |
| 0.7 | 2.429 | 22.016 |
| 0.8 | 2.776 | 22.016 |
| 0.9 | 3.123 | 22.016 |
| 1.0 | 3.470 | 22.016 |
| 1.1 | 3.817 | 22.016 |
| 1.2 | 4.164 | 22.016 |

## 3. Results and Discussion

### 3.1. Mesh Convergence Analysis

Results for thrust, torque, and effectiveness for coarse, medium, and fine mesh in three advanced coefficients (*J*) are offered to improve prediction. The propeller's grid dependence is chosen in order to produce superior simulation results compared to the experimental.

In the presented case study, using three grids and the grid refinement ratio $rG = \sqrt{2}$ (the value advised by ITTC [22]), mesh convergence research is carried out at advance coefficient *J* = 0.6. With cell counts of 1.38, 3.52, and 6.89 million, three meshes coarse, medium, and fine are produced. The following definitions describe the solution differences between two simulations at Eq. 10, such as fine-medium $\varepsilon_{12}$ and medium-coarse$\varepsilon_{23}$:

$$\varepsilon_{12} = \frac{S_1 - S_2}{S_1}; \varepsilon_{23} = \frac{S_2 - S_3}{S_2} \quad (10)$$

Where: $S_1$, $S_2$, $S_3$, the output of the simulation of open water using fine, medium, and coarse mesh.

The finding of the mesh convergence investigation is displayed in Table 3. Particularly for $K_T$ , which changed from 0.25% to 1.71%, the variations in solution from coarse mesh to fine mesh are particularly considerable. The same behavior is also displayed by $K_Q$ and $\eta_O$. It indicates that the solution converged on a value by enlarging the mesh size. Therefore, for further calculation in this instance, fine mesh should be employed.

Table 3. Results of mesh convergence study at *J* = 0.60

| Characteristics | Mesh density | | | $\varepsilon_{21}$ [%] | $\varepsilon_{32}$ [%] |
|---|---|---|---|---|---|
| | Coarse grids | Medium grids | Fine grids | | |
| $K_T$ | 0.2808 | 0.2760 | 0.2753 | 0.25 | 1.71 |
| $K_Q$ | 0.0523 | 0.0510 | 0.0509 | 0.39 | 2.49 |

| Characteristics | Mesh density | | | $\varepsilon_{21}$ [%] | $\varepsilon_{32}$ [%] |
|---|---|---|---|---|---|
| | Coarse grids | Medium grids | Fine grids | | |
| $\eta_O$ | 0.5130 | 0.5170 | 0.5164 | 0.14 | 0.79 |

### 3.2. Calculation Results

The comparison of simulation in mesh fine and experimental data for the propeller's open water characteristics at advanced velocities $J$ ranging from 0.0 to 1.2 is shown in Table 4. The variations between the CFD (Computational Fluid Dynamics) simulation, $S$, and the EFD (Experimental Fluid Dynamics), $D$ data are defined at Eq. 11 by:

$$E\% = \frac{D-S}{D} 100\% \quad (11)$$

The simulation results indicate good agreement with the experimental findings when the computational results and experimental data from are examined.

Table 4. Result of open water simulation compared to experimental.

| J | Thrust Coefficient ($K_T$) | | | 10 Torque Coefficient (10 $K_Q$) | | | Efficiency ($\eta$) | | |
|---|---|---|---|---|---|---|---|---|---|
| | EFD | CFD | $E$(%) | EFD | CFD | $E$(%) | EFD | CFD | $E$(%) |
| 0.0 | 0.511 | 0.496 | 2.9 % | 0.850 | 0.840 | 1.0 % | 0.000 | 0.000 | 0 % |
| 0.1 | 0.489 | 0.471 | 1.6 % | 0.818 | 0.801 | 2.1 % | 0.095 | 0.093 | 2.1% |
| 0.2 | 0.451 | 0.442 | 1.9 % | 0.772 | 0.756 | 1.5 % | 0.186 | 0.186 | 0% |
| 0.3 | 0.405 | 0.404 | 2.0 % | 0.715 | 0.700 | 2.6 % | 0.271 | 0.276 | -1.8% |
| 0.4 | 0.364 | 0.364 | 0 % | 0.654 | 0.639 | 1.5 % | 0.354 | 0.363 | -2.2% |
| 0.5 | 0.319 | 0.321 | -0.6 % | 0.590 | 0.576 | 2.4 % | 0.430 | 0.443 | -3.0% |
| 0.6 | 0.270 | 0.275 | -1.8 % | 0.524 | 0.509 | 2.7 % | 0.492 | 0.516 | -4.8% |
| 0.7 | 0.215 | 0.227 | -2.7 % | 0.454 | 0.439 | 1.6 % | 0.552 | 0.577 | -4.5% |
| 0.8 | 0.179 | 0.182 | -4.0 % | 0.387 | 0.373 | 1.4 % | 0.592 | 0.620 | -4.6% |
| 0.9 | 0.103 | 0.132 | -5.6 % | 0.314 | 0.299 | 2.5 % | 0.591 | 0.632 | -5.9% |
| 1.0 | 0.058 | 0.082 | -12.3 % | 0.234 | 0.220 | 1.4 % | 0.564 | 0.592 | -4.9% |
| 1.1 | 0.021 | 0.030 | -5.2 % | 0.144 | 1.131 | 2.3 % | 0.340 | 0.394 | -4.5% |
| 1.2 | 0.00 | 0.00 | 0% | 0.00 | 0 | 0% | 0.00 | 0.00 | 0% |

The Diagram open water test of simulation and experimental are shown in Figures 7 and 8. Figures 9 and 10 display the pressure distribution on the propeller suction side, meanwhile, Figures 11 and 12 display the axial velocity of the open water test at $J$=0.6 with coarse and fine meshes With a higher advance coefficient $J$, the flow becomes more turbulent as the axial velocity rises. This is because, while the rotational speed ($n$) and propeller diameter ($D$) are constant, the advance coefficient ($J$) and advance velocity ($va$) have a linear connection.

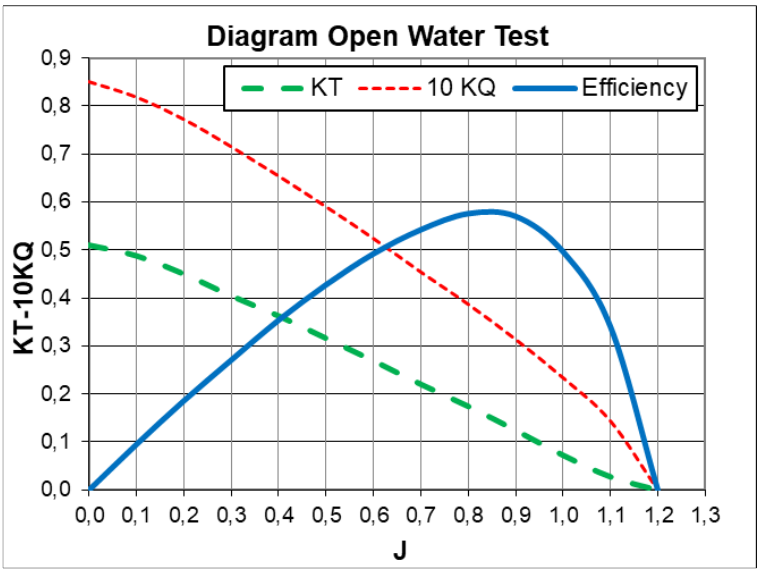


Figure 7. Diagram open water test (EFD).

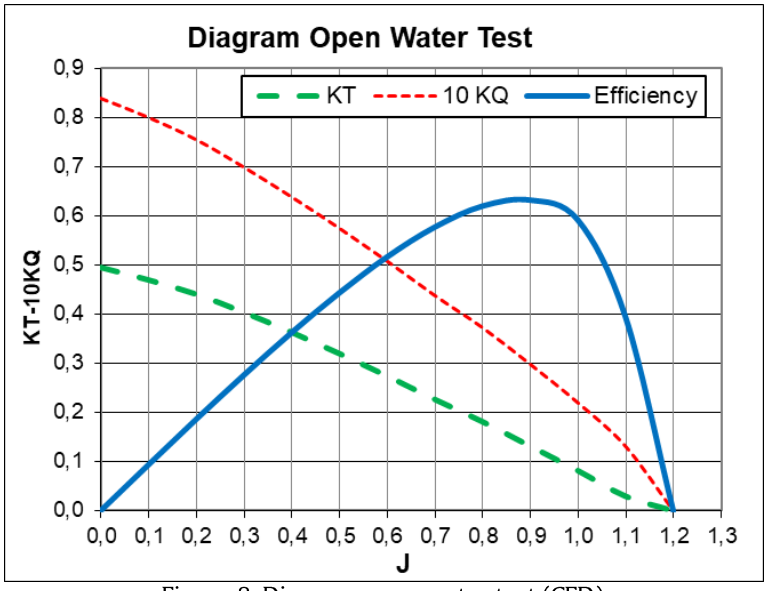


Figure 8. Diagram open water test (CFD).

.

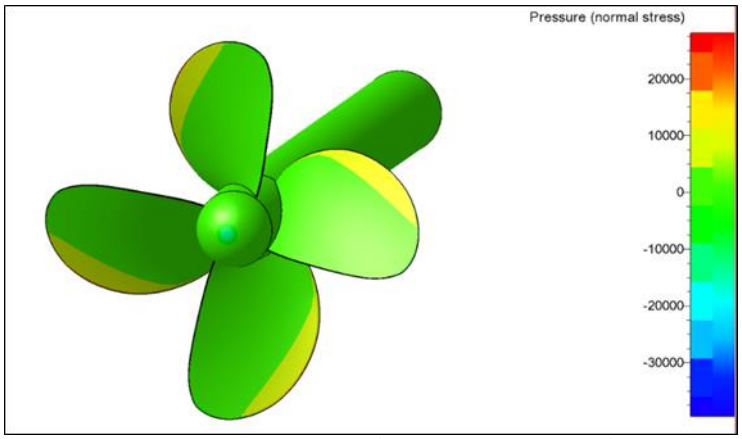


Figure 9. Pressure distribution at course mesh.

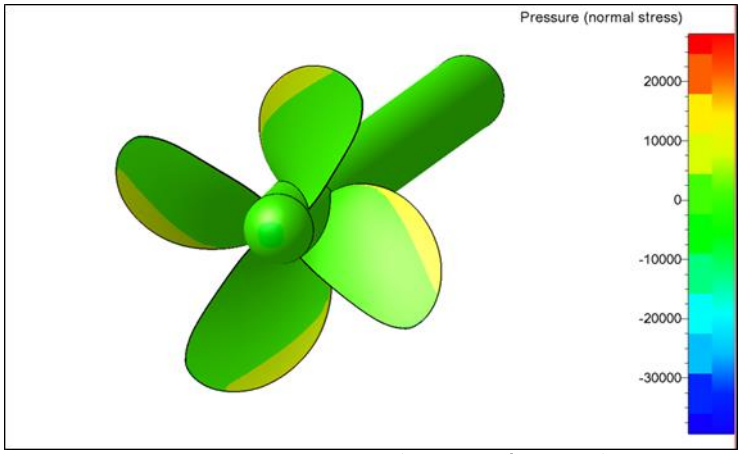


Figure 10. Pressure distribution at fine mesh.

.

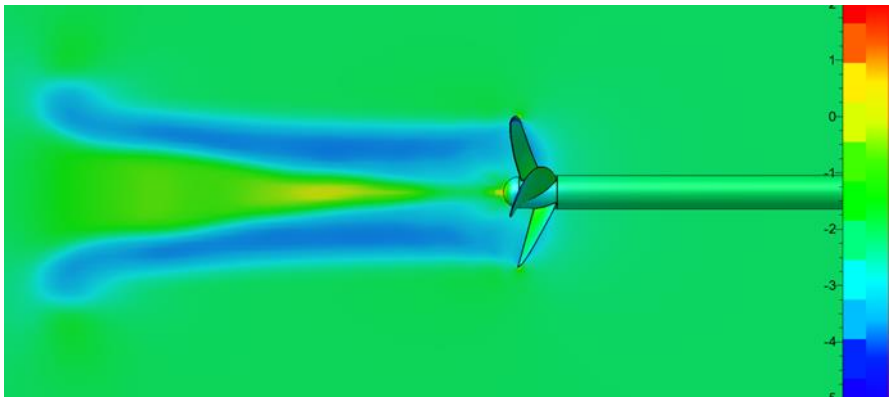

Figure 11. The axial velocity distribution (coarse mesh).

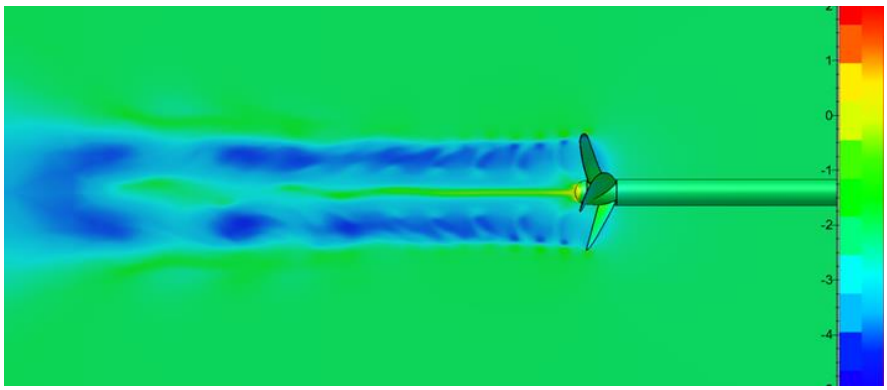

Figure 12. The axial velocity distribution (fine mesh).

Base on Figures 7- 8 and Table 3, show that the CFD result and experimental result are very similar, particularly in terms of open water efficiency. The difference in open water efficiency is only approximately under 5%. Studying mesh convergence models are factors that led to successful results.

## 4. Conclusion

The CFD approach has been used in this study to forecast the propeller open water characteristics for open water research. Various numerical simulations of the B-series propeller to determine the hydrodynamic force based on modifications in the advance velocity (*Va*) at fine mesh. Research on mesh convergence is conducted with an advance coefficient of $J = 0.6$ with three meshes coarse, medium, and fine. The outcomes are very consistent with the outcome of the experiment. This demonstrates the critical importance of mesh convergence analysis and mesh refining for crucial regions of propeller blades. This study demonstrates the CFD method's capacity to obtain the best performance of open water. In General, the characteristics of the marine propeller in open water are positively impacted by different advanced velocities. These CFD data can therefore be used to provide a rough prediction of propeller performance. Considering this research' s findings, further study is necessary to investigate verification, validation and the uncertainty analysis of open water tests of this type of propeller.

## Acknowledgment

This study was supported by a research grant from the National Research and Innovation Agency as a sponsor of research-based education programs number: SP/112/BPPT/08/2021. The authors would like to thank the Indonesian Hydrodynamics Laboratory and colleagues who have assisted with the research and supported to finish of this paper.

## References

[1] M. F. Islam and F. Jahra, " Improving Accuracy and Efficiency of CFD Predictions of Propeller Open Water Performance" , Journal of Naval Architecture and Marine Engineering, Vol.16, pp. 1-20, 2019.

[2] A. Fitriadhya, N. A. Adamb, W. S. Kongc, F, Mahmuddind, and C. J. Quahe, " Prediction of Propeller Performance using Computational Fluid Dynamics Approach" , EPI International Journal of Engineering, Vol. 2 No. 2, pp. 185-193, 2019. doi: 10.25042/epi-ije.082019.15.

[3] A. F. N. Oloan, I. M. Ariana, and A. Baidowi, " Open Water and Performance Analysis of Marine Propeller with PBCF Based CFD Method" , IOP Conf. Series: Earth and Environmental Science Vol. 972, No. 012050, 2022. doi:10.1088/1755-1315/972/1/01205.

[4] A. Fitriadhy, N. A. Adam, C.J. Quah, J. Koto, and F. Mahmuddin," CFD Prediction of B-Series Propeller Performance in Open Water" , CFD Letters, Vol. 12, Issue. 2, pp. 58-68 2020.

[5] M.S. Baital and I.K.A.P Utama, " CFD Analysis into the Drag Estimation of Smooth and Roughened Surface Due to Marine Biofouling" , IPTEK, the Journal for Technology and Science, Vol. 28, No. 3, 2017.

[6] C. G. Grlj, N. Degiuli, A. Farkas and I. Martic, " Numerical Study of Scale Effects on Open Water Propeller Performance" , Journal of Marine Science and Engineering, Vol.10, pp. 1132, 2022, doi: 10.3390/jmse10081132.
[7] L. Savio and K. Koushan, " Open Water Characteristics of Three ModelScale Flexible Propellers" , VIII International Conference on Computational Methods in Marine Engineering, MARINE 2019.
[8] W. Herucakra, L.P. Adnyani and L. Megantoro, " Integrity Assessment of Wall Distorted of Buried Gas Pipeline" , Kapal: Jurnal Ilmu Pengetahuan danTeknologi Kelautan, Vol. 20 No. 1, pp. 1-15, 2023.
[9] D.A. Putri, M.H.N. Aliffrananda, S. Riyadi, S. Sutiyo, and I.K.A.P. Utama, " Numerical Analysis on Added Resistance of a Crew Boat with Variation of Wave Period" , Kapal: Jurnal Ilmu Pengetahuan danTeknologi Kelautan, Vol. 20 No. 1, pp. 16-26, 2023. doi :10.14710/kapal.v20i1.48615
[10] M.R. Utina, Rina, E. Suwarni, P. Virliani, Widodo, D. Purnamasari, " Numerical Analysis of Submarine Hydrodynamic Force Near the Seabed" , Kapal: Jurnal Ilmu Pengetahuan danTeknologi Kelautan, Vol. 20 No. 1, pp. 27-33, 2023, doi: 10.14710/kapal.v18i3.41010
[11] T. N. Tu, " Numerical simulation of propeller open water characteristics using RANSE method," Alexandria Engineering Journal, Vol.58, pp. 531-537, 2019. doi:10.1016/j.aej.2019.05.005
[12] M. Zhao, W. Zhao, and D. Wan, " Numerical simulations of propeller cavitation flows based on OpenFOAM" , Journal of Hydrodynamics, 2020, doi:10.1007/s42241-020-0071-8
[13] X. Zhou, C. Liu, H. Ren, and C. Xu, " Numerical Analysis of Propeller-Induced Hydrodynamic Interaction between Ships" , Journal of Marine Science and Engineering, Vol.11, pp. 537, 2023. doi:10.3390/jmse11030537
[14] L. He and S. A. Kinnas, " Numerical simulation of unsteady propeller/rudder interaction" , International Journal of Naval Architecture and Ocean Engineering, Vol. 9, pp. 677-692, 2017. doi:10.1016/j.ijnaoe.2017.02.004
[15] H.Jasak, V. Vukcevic, I. Gatin and I. Lalovic, " CFD validation and grid sensitivity studies of full-scale ship self-propulsion" , International Journal of Naval Architecture and Ocean Engineering, Vol. 11, pp. 33-43, 2019. doi:10.1016/j.ijnaoe.2017.12.004
[16] L. Wang, C. Guo, Y. Su, P. Xu, and T. Wu, " Numerical analysis of a propeller during heave motion in the cavitating flow" , Applied Ocean Research, Vol.66, pp.131– 145, 2017. doi:10.1016/j.apor.2017.05.001
[17] W. Zhang, C. Chen, Z. Wang, Y. Li, H. Guo, J. Hu, H. Li and C. Guo, " Numerical simulation of structural response during propeller-rudder interaction" , Engineering Applications of Computational Fluid Mechanics, Vol. 15, No.1, pp. 584– 612, 2021. doi:10.1080/19942060.2021.1899989
[18] J. Hu, W. Zhang, S. Sun, and C. Guo, " Numerical simulation of Vortex– Rudder interactions behind the propeller" , Ocean Engineering, Vol. 190, pp. 106446, 2019. doi:10.1016/j.oceaneng.2019.106446
[19] F. Liao, X. Yang, S. Wang, and G. He, " Grid-dependence study for simulating propeller crash back using large-eddy simulation with immersed boundary method" , Ocean Engineering, Vol. 218, pp. 108211, 2020. doi:10.1016/j.oceaneng.2020.108211
[20] A. Posa, R. Broglia, M. Felli, M. Falchi, and E. Balaras, " Characterization of the wake of a submarine propeller via Large-Eddy Simulation" , Computers & Fluids, Vol. 184, pp. 138-152, 2019. doi:10.1016/j.compfluid.2019.03.011
[21] B. Zhang, C. Ding, and C.Liang, " High-Order Implicit Large-Eddy Simulation of Flow over a Marine Propeller" , Computers & Fluids, Vol. 224, pp. 104967, 2021. doi:10.1016/j.compfluid.2021.104967
[22] ITTC – Recommended Procedures and Guidelines, " Uncertainty Analysis in CFD Verification and Validation Methodology and Procedures" , 7.5-03-01-01, 2008.